### VERY HIGH COLUMN DENSITY AND SMALL REDDENING TOWARD GRB 020124 AT $z = 3.20^{1}$

J. Hjorth,<sup>2</sup> P. Møller,<sup>3</sup> J. Gorosabel,<sup>4,5,6</sup> J. P. U. Fynbo,<sup>2,7</sup> S. Toft,<sup>2</sup> A. O. Jaunsen,<sup>8</sup> A. A. Kaas,<sup>9</sup> T. Pursimo,<sup>9</sup> K. Torii,<sup>10</sup> T. Kato,<sup>11</sup> H. Yamaoka,<sup>12</sup> A. Yoshida,<sup>10,13</sup> B. Thomsen,<sup>7</sup> M. I. Andersen,<sup>14</sup> I. Burud,<sup>6</sup> J. M. Castro Cerón,<sup>15</sup> A. J. Castro-Tirado<sup>5</sup> A. S. Fruchter,<sup>6</sup> L. Kaper,<sup>16</sup> C. Kouveliotou,<sup>17</sup> N. Masetti,<sup>18</sup> E. Palazzi,<sup>18</sup> H. Pedersen,<sup>2</sup> E. Pian,<sup>19</sup> J. Rhoads,<sup>6</sup> E. Rol,<sup>16</sup> N. R. Tanvir,<sup>20</sup> P. M. Vreeswijk,<sup>8</sup> R. A. M. J. Wijers,<sup>16</sup> and E. P. J. van den Heuvel<sup>16</sup> Received 2003 March 28; accepted 2003 July 16

#### **ABSTRACT**

We present optical and near-infrared observations of the dim afterglow of GRB 020124, obtained between 2 and 68 hr after the gamma-ray burst. The burst occurred in a very faint  $(R \gtrsim 29.5)$  damped Ly $\alpha$  absorber (DLA) at a redshift of  $z = 3.198 \pm 0.004$ . The derived column density of neutral hydrogen is  $log(N_{\rm H\,I}) = 21.7 \pm 0.2$ , and the rest-frame reddening is constrained to be E(B-V) < 0.065, i.e.,  $A_V < 0.20$  for standard extinction laws with  $R_V \approx 3$ . The resulting dust-to-gas ratio is less than 11% of that found in the Milky Way but consistent with the SMC and high-redshift QSO DLAs, indicating a low metallicity and/or a low dust-to-metal ratio in the burst environment. A gray extinction law (large  $R_{\nu}$ ), produced through preferential destruction of small dust grains by the gamma-ray burst, could increase the derived  $A_V$  and dust-to-gas ratio. The dimness of the afterglow is, however, fully accounted for by the high redshift: if GRB 020124 had been at z = 1, it would have been approximately 1.8 mag brighter—in the range of typical bright afterglows.

Subject headings: cosmology: observations — dust, extinction — galaxies: abundances galaxies: ISM — gamma rays: bursts

#### 1. INTRODUCTION

Spectroscopy of the optical afterglows of cosmological gamma-ray bursts (GRBs) allows detailed studies of the chemical and kinematical properties of gas along the lines of sight. Independently of the brightness of the host galaxy, the resulting insight into the GRB environment and its dust and gas content can provide clues to the nature of GRB progenitors, as well as the properties of high-redshift galaxies. In particular, constraints on the column density of neutral hydrogen, N(H I), can be obtained through Ly $\alpha$  absorption if the burst is sufficiently distant to redshift the Ly $\alpha$  line into the near-UV/optical domain. Unlike X-ray studies, where one infers N(H I) only indirectly on the basis of an assumed metallicity, the derived N(H I) will be independent of metallicity.

In this regard, spectroscopy of GRB optical afterglows bears some resemblance to that of damped Ly $\alpha$  absorbers (DLAs; Wolfe et al. 1986), which are gas-rich absorption systems intervening the lines of sight to background sources, such as QSOs. DLAs are chemically enriched and are therefore most likely caused by gas in, or close to, galaxies (e.g., Lu et al. 1996 and references therein; Pettini et al. 1997b). In some cases galaxy counterparts of DLAs have been detected directly (Møller & Warren 1993, 1998; Djorgovski et al. 1996; Fynbo, Møller, & Warren 1999;

<sup>2</sup> Astronomical Observatory, University of Copenhagen, Juliane Maries Vej 30, DK-2100 Copenhagen Ø, Denmark; jens@astro.ku.dk. <sup>3</sup> European Southern Observatory, Karl-Schwarzschild-Strasse 2, D-85748 Garching bei München, Germany.

<sup>&</sup>lt;sup>1</sup> Based on observations with the Nordic Optical Telescope, which is operated on the island of La Palma jointly by Denmark, Finland, Iceland, Norway, and Sweden, at the Spanish Observatorio del Roque de los Muchachos of the Instituto de Astrofísica de Canarias, and on observations collected by the Gamma-Ray Burst Collaboration at ESO (GRACE) at the European Southern Observatory, Paranal, Chile (ESO Large Programme 165.H-0464).

<sup>&</sup>lt;sup>4</sup> Danish Space Space Research Institute, Juliane Maries Vej 30, DK-2100 Copenhagen Ø, Denmark.

<sup>&</sup>lt;sup>5</sup> Instituto de Astrofísica de Andalucía (IAA-CSIC), Apartado 3.004, E-18080 Granada, Spain.

<sup>&</sup>lt;sup>6</sup> Space Telescope Science Institute, 3700 San Martin Drive, Baltimore, MD 21218.

<sup>&</sup>lt;sup>7</sup> Department of Physics and Astronomy, University of Aarhus, DK-8000 Århus C, Denmark.

<sup>&</sup>lt;sup>8</sup> European Southern Observatory, Casilla 19001, Santiago 19, Chile.

<sup>&</sup>lt;sup>9</sup> Nordic Optical Telescope, Apartado 474, E-38700 St. Cruz de La Palma, Canary Islands, Spain.

<sup>&</sup>lt;sup>10</sup> Cosmic Radiation Laboratory, RIKEN, 2-1, Hirosawa, Wako 351-0198, Japan.

<sup>&</sup>lt;sup>11</sup> Department of Astronomy, Kyoto University, Sakyo-ku, Kyoto 606-8502, Ĵapan.

<sup>&</sup>lt;sup>12</sup> Department of Physics, Faculty of Science, Kyushu University, Chuo-ku, Fukuoka 810-8560, Japan.

<sup>&</sup>lt;sup>13</sup> Department of Physics, Aoyama Gakuin University, 6-16-1, Chitosedai, Setagaya 157-8572, Japan.

<sup>&</sup>lt;sup>14</sup> Astrophysikalisches Institut Potsdam, D-14482 Potsdam, Germany.

 <sup>&</sup>lt;sup>15</sup> Real Instituto y Observatorio de la Armada, Sección de Astronomía, 11.110 San Fernando-Naval (Cádiz), Spain.
 <sup>16</sup> Astronomical Institute "Anton Pannekoek," NL-1098 SJ Amsterdam, Netherlands.
 <sup>17</sup> Universities Research Association, Marshall Space Flight Center (NASA), Huntsville, AL 35812.

<sup>&</sup>lt;sup>18</sup> IASF/CNR, Sezione di Bologna, Via Gobetti 101, I-40129 Bologna, Italy.

<sup>&</sup>lt;sup>19</sup> INAF, Osservatorio Astronomico di Trieste, via Tiepolo, I-34131 Trieste, Italy.

<sup>&</sup>lt;sup>20</sup> Department of Physical Sciences, University of Hertfordshire, College Lane, Hatfield, Hertfordshire AL10 9AB, UK.

Møller et al. 2002). The important and interesting difference between QSO DLAs and GRB absorption systems is that the lines of sight through QSO DLAs are absorption cross section—selected, whereas GRB absorbers (at the GRB redshift) are "GRB progenitor site"—selected. Therefore, GRB absorbers are likely to probe sight lines through different parts of DLA galaxies than QSO absorbers do and hence contribute to a more complete picture of the properties of high-redshift galaxies.

The dust content of DLAs has been constrained mainly by two methods: (1) by comparing the colors of background QSOs having intervening DLAs with the colors of a control sample of QSOs without intervening DLAs (Pei, Fall, & Bechtold 1991), and (2) by studying the metal abundance ratios, most notably Zn versus Si and iron group elements, and inferring the dust depletion by comparison with interstellar clouds in the Galaxy (Lu et al. 1996; Kulkarni, Fall, & Truran 1997; Pettini et al. 1997a; Ledoux, Bergeron, & Petitjean 2002). The main conclusion of these studies is that DLAs in general are metal-poor and that the fraction of the metals bound in dust grains is roughly the same as, or somewhat lower than, that found in the Galaxy.

This paper presents optical/near-IR photometry and optical spectroscopy of the afterglow of GRB 020124. GRB 020124 (burst trigger on 2002 January 24.44531 UT) was the second *HETE-2* burst (Ricker et al. 2002) to be localized to arcsecond precision and is the only burst for which a host galaxy has not been detected when searched for with the Hubble Space Telescope (HST; Berger et al. 2002; Bloom, Kulkarni, & Djorgovski 2002). We determine the redshift of the burst to be 3.20, which is the fourth highest redshift known for a GRB to date and the third highest after GRB 000131 at z = 4.50 (Andersen et al. 2000) and GRB 030323 at z = 3.37 (Vreeswijk et al. 2003b) on the basis of afterglow absorption lines rather than host-galaxy emission lines. We also show that it has a very high column density, qualifying it as a DLA [the highest value of N(H I) of known GRB afterglows and higher than almost all QSO DLAs]. We discuss the implications for the dust-to-gas ratio of the GRB surroundings, including the effects of metallicity and destruction of dust by the GRB itself.

We assume a cosmology where  $H_0 = 70 \text{ km s}^{-1} \text{ Mpc}^{-1}$ ,  $\Omega_m = 0.3$ , and  $\Omega_{\Lambda} = 0.7$ . For these parameters, a redshift of 3.20 corresponds to a luminosity distance of 27.47 Gpc and

a distance modulus of 47.19. One arcsecond corresponds to 7.55 proper kiloparsec, and the look-back time is 11.5 Gyr.

#### 2. OBSERVATIONS

The observing log and photometric results are reported in Table 1 and summarized below.

### 2.1. Optical Imaging

The position of the burst was observed at RIKEN with the 0.25 m f/3.4 hyperboloid astrograph equipped with unfiltered CCD camera AP7p. The field of view was  $50'\times50'$ , which covered the entire 12' radius HETE-2 error circle (Ricker et al. 2002). The observation started on January 24.530 UT; 126 frames of 20 s exposure were acquired by January 24.574 UT. Point-spread function photometry was applied to each of the 126 frames. The resultant photometric measurements were combined to yield a 3.0  $\sigma$  detection at the position of the afterglow reported by Berger et al. (2002).

R-band images of the optical afterglow were obtained with StanCam at the 2.56 m Nordic Optical Telescope (NOT) between January 26.035 and January 26.076 2002 UT. I-band images were obtained at VLT-Melipal (UT3) between January 26.311 and 26.318 UT. R-band images were obtained with FORS1 on VLT-Melipal between January 27.278 UT and 27.292 UT. The latter images have a pronounced background pattern due to instrument reflections of the very bright background (the Moon was ~75% illuminated). The variation in the pattern across the field is approximately 3%-4%. To flatten each individual image we used SExtractor to create a smoothed background image that was subsequently subtracted. The five background-subtracted images were then combined.

All images were preprocessed using standard tools and calibrated using nearby comparison stars from the field photometry of Henden (2002). The derived magnitudes are listed in Table 1.

### 2.2. Near-Infrared Imaging

Near-IR observations were obtained with ISAAC on VLT-Antu (UT1). The data consist of a total of 30 minutes in the  $K_s$  band and 30 minutes in the  $J_s$  band obtained on January 26.2 UT and 30 minutes in the  $K_s$ 

 ${\it TABLE \ 1} \\ {\it Log of Observations and Photometry of the Afterglow of GRB \, 020124}$ 

Date (2002 Jan UT)	Filter <sup>a</sup> /Grism	Exposure Time (s)	Telescope <sup>b</sup>	FWHM <sup>c</sup> (arcsec)	Brightness <sup>d</sup> (mag)
24.55	Unfiltered	126 × 20	RIKEN	2.2	$18.5^{+0.4}_{-0.3}$
26.04	R	$6 \times 600$	NOT	1.14	$23.42 \pm 0.25$
26.20	$K_s$	$30 \times 60$	Antu	0.50	$20.55 \pm 0.13$
26.23	$J_{\scriptscriptstyle S}$	$20 \times 90$	Antu	0.68	$21.94 \pm 0.16$
26.32	$\widetilde{I}$	$2 \times 60 + 120$	Melipal	0.74	$22.94 \pm 0.15$
26.34	300V	$2 \times 600$	Melipal	1.2	
27.20	$K_{\rm s}$	$30 \times 60$	Antu	0.56	$21.92^{+0.37}_{-0.28}$
27.28	R	$5 \times 180$	Melipal	0.66	$24.26^{+0.45}_{-0.32}$

<sup>&</sup>lt;sup>a</sup> The broadband optical (*R*, *I*) filters used were Bessel filters (Bessel 1990).

<sup>&</sup>lt;sup>b</sup> RIKEN represents a 0.25 m f/3.4 hyperboloid astrograph (Wako, Saitama, Japan) equipped with an unfiltered CCD camera; NOT is the 2.56 m Nordic Optical Telescope (La Palma, Canary Islands, Spain) equipped with StanCam; Antu and Melipal are the 8.2 m Unit Telescopes 1 and 3 on ESO's VLT at Paranal Observatory, Chile, equipped with ISAAC and FORS1, respectively.

<sup>&</sup>lt;sup>c</sup> Measured seeing FWHM of pointlike objects in the field.

d Uncorrected for Galactic extinction. The brightnesses are reported as  $R_C$ ,  $I_C$ , J, and  $K_s$  magnitudes.

band obtained on January 27.2 UT. The reduction was carried out with the ECLIPSE software package (Devillard 1997) and the IRAF Experimental Deep Infrared Mosaicing Software xdimsum. ECLIPSE was used to remove effects of electrical ghosts from science and calibration frames and to construct flat fields and bad-pixel maps from a series of twilight-sky flats. Sky subtraction and combination of the dithered science frames were carried out with xdimsum. To account for the rapidly varying background, the sky value in each pixel was calculated as the running median of the pixel value in the exposures taken immediately before and after a given exposure. To minimize the effects on the running median of bright objects in neighboring frames, the subtraction was carried out in two iterative steps: First, a cosmic-ray-cleaned, background-subtracted combined image was constructed, from which a mask of all the objects was created. This mask was then registered to the individual frames and taken into account in the following running-median background subtraction. Residual background signatures were subsequently removed by fitting high-order polynomials to the rows and columns of the individual (masked) frames. Finally, the individual background-subtracted images were registered and mediancombined. Excerpts of the resulting images are shown in Figure 1.

Photometric calibration to J and  $K_s$  magnitudes was performed using standard-star observations of 9106/S301-D and 9149/S860-D (Persson et al. 1998) on the nights of observation. The images were astrometrically calibrated using comparison stars from the Guide Star Catalogue II (GSC-II)<sup>21</sup> using the WCStools software package by

21 The Guide Star Catalogue II is a joint project of the Space Telescope Science Institute and the Osservatorio Astronomico di Torino. Space Telescope Science Institute is operated by the Association of Universities for Research in Astronomy, for the National Aeronautics and Space Administration under contract NAS 5-26555. The participation of the Osservatorio Astronomico di Torino is supported by the Italian Council for Research in Astronomy. Additional support is provided by European Southern Observatory, Space Telescope European Coordinating Facility, the International GEMINI project and the European Space Agency Astrophysics Division.

D. Mink.<sup>22</sup> The absolute astrometry has an rms of 0."43 in the  $K_s$  band. The resulting coordinates of the infrared afterglow of GRB 020124 are R.A. =  $09^{\rm h}32^{\rm m}50.82$ , decl. =  $-11^{\circ}31'11.0'$  (J2000.0), consistent with the position of the radio and optical afterglow (Berger et al. 2002).

# 2.3. Spectroscopy

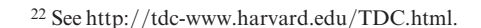
Spectroscopic observations were obtained on January 26.3 with FORS1 on VLT-Melipal using the 300V+10 grism and the order-separation filter GG375 in long-slit mode with a 1".0 wide slit. This configuration provides a wavelength coverage 3650–7500 Å at a resolution of 13 Å. The total integration time was 1200 s, evenly divided between two exposures. Standard data reduction procedures were performed using MIDAS. The two separate exposures allowed us to reliably reject cosmic-ray events before co-addition. The spectrophotometric standard LTT9491 (Hamuy et al. 1994) was observed using the same configuration.

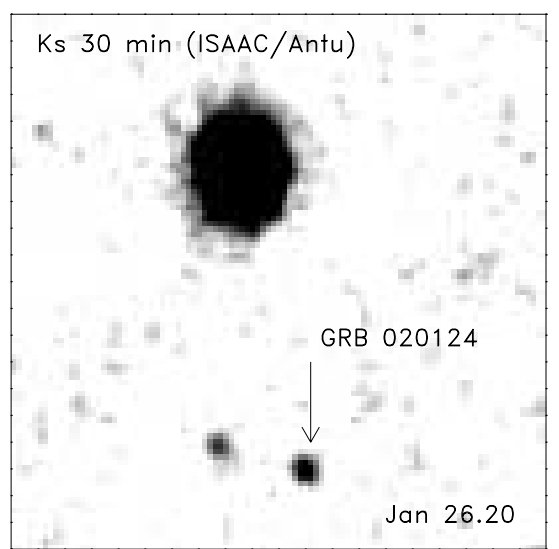
#### 3. RESULTS

# 3.1. Spectral Energy Distribution: Spectral Index and Redshift Estimate

The extracted, flux-calibrated spectrum is shown in Figure 2. Because of the faintness of the object spectrum and the resulting dominance of systematic errors from sky subtraction close to bright airglow lines, the signal-to-noise ratio fluctuates rapidly in the red part of the spectrum. What may look like absorption or emission features redward of 5500 Å should therefore not be trusted. The strong absorption line around 5100 Å is clearly significant, and several other absorption features blueward of 5500 Å are marginally significant at the 3–4  $\sigma$  level.

One or more of the absorption lines seen in the blue part of Figure 2 could be due to Ly $\alpha$ , which would indicate a redshift in excess of 2.3. Our first objective was therefore to construct the spectral energy distribution (SED) in the optical to determine its slope and to look for possible large-scale





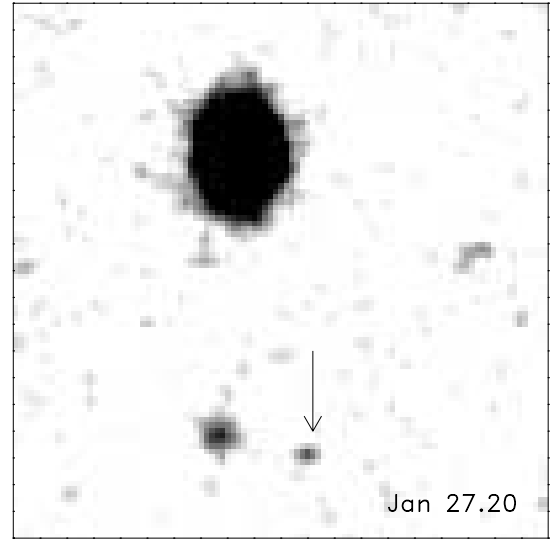


Fig. 1.— $K_s$  images obtained with ISAAC on 2002 January 26.20 UT (*left*) and 27.20 UT (*right*) of GRB 020124, marked by an arrow. The images are  $15'' \times 15''$ . North is up, and east is to the left.

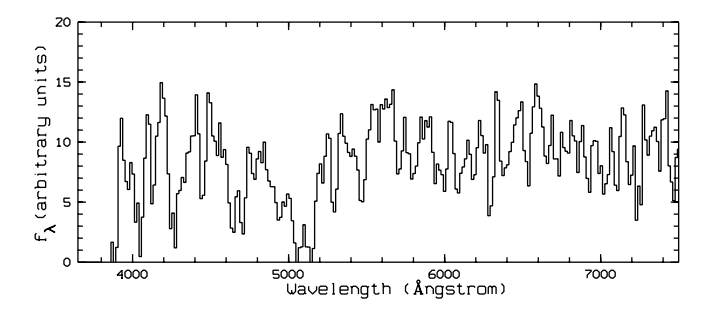


Fig. 2.—Extracted, flux-calibrated FORS1 300V spectrum of GRB 020124 obtained on 2002 January 26.34 UT. The ordinate is  $f_{\lambda}$  in arbitrary units. From 4000 to 5500 Å the signal-to-noise ratio per resolution element (13 Å) in the continuum grows from 1.8 to 3.5. Longward of 5500 Å the signal-to-noise ratio is completely dominated by sky-subtraction errors and therefore varies rapidly from pixel to pixel. In order to obtain the best possible value for the spectral slope of the spectrum, we have identified "good" sections of the spectrum as detailed in § 3.1 and shown in Fig. 3.

signatures (spectral drops) that might indicate the onset of the Lyman forest and/or the Lyman valley as expected in an object with redshift significantly in excess of 2.3. For this purpose we carefully defined a series of intervals along the spectrum where systematic errors from night-sky emission-line subtraction did not pose any problems. The total number of counts was determined in each interval of the afterglow spectrum, as well as of the spectrum of the spectrophotometric standard. Uncertainties were calculated directly via propagation of photon statistics.

The resulting fluxes and corresponding uncertainties (after correction for air mass) in each bin are plotted in Figure 3. In Figure 3a the minimum- $\chi^2$  pure power-law fit  $(f_{\nu} \propto \nu^{-\beta}; \ \beta = 2.36 \pm 0.23; \ \text{reported uncertainties are 1 } \sigma$ errors throughout this paper) is overplotted but is seen to be a very poor fit to the data points. In particular, the data point at 5100 Å falls many standard deviations below any power-law fit. Such a large drop in that wide a bin can effectively be caused only by a damped Ly $\alpha$  line at a redshift of about 3.2. At this redshift one expects to see not only the Ly $\alpha$  line but also a significant drop due to the Lyman forest and the signature of the onset of the red slope of the Lyman valley (Møller & Jakobsen 1990). In Figure 3b we therefore plot the same data points, but here we overlay a model power law including the predicted absorption due to the intervening intergalactic medium at z = 3.2. The power law again represents the minimum- $\chi^2$  fit and has an index of  $\beta=1.32\pm0.25$ . Comparing the  $\chi^2$  of the fits in Figures 3aand 3b, we find that even if we ignore the presence of the Ly $\alpha$  line (i.e., consider only the large-scale SED), the z = 3.2 model SED represents an acceptable fit, while the pure power law is rejected at the 98.6% confidence level  $(\Delta \chi^2 = 16.4 \text{ for } 20 \text{ degrees of freedom [dof]}).$ 

# 3.2. Redshift and H I Column Density of the Ly $\alpha$ Line

Following the determination of the underlying power-law index and approximate redshift, we proceeded to fit the Ly $\alpha$  line itself. The part of the spectrum useful for line-fitting is shown again in Figure 4, here normalized by division with the fitted power law. Overplotted are model absorption spectra with z=3.198. The model spectra include the Lyman series, Si II, Si III, and O I lines. On the blue side of the Ly $\alpha$  line we see the expected line-blanketing by the Lyman forest. At this resolution, lines in the Lyman forest

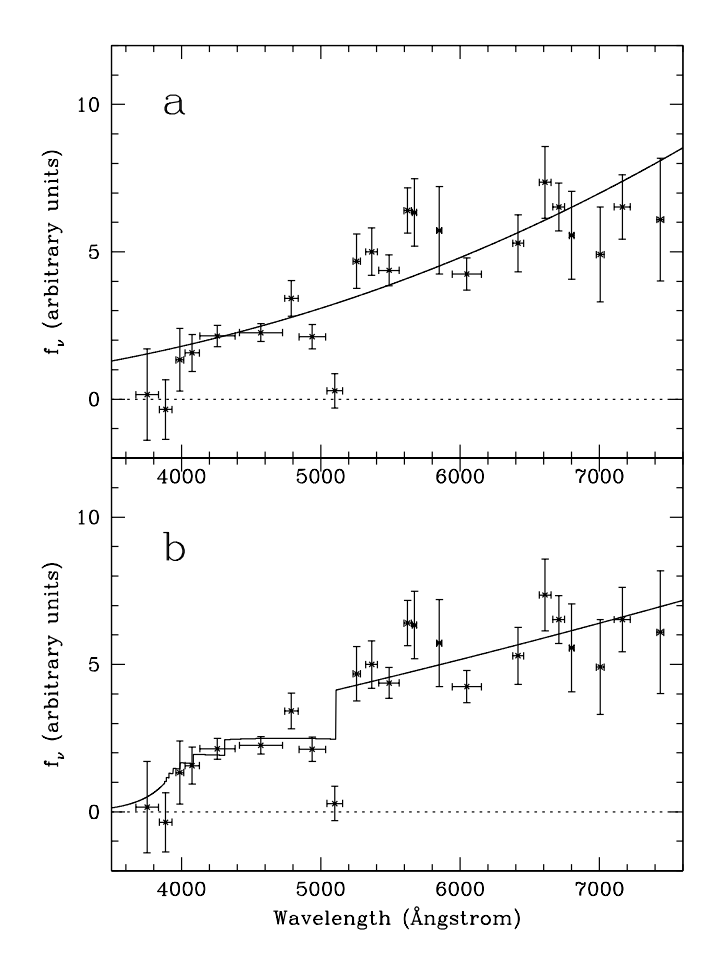


Fig. 3.—Spectrum of GRB 020124 (Fig. 2) summed in bins free from strong sky lines. (a) A pure power law does not provide an acceptable fit mostly because of the strong absorption line at 5100 Å. This strong absorption feature can be explained only by a damped Ly $\alpha$  line close to z=3.2. A power-law fit to the data excluding the bin at 5100 Å leads to a spectral slope of  $\beta=2.36\pm0.23$  incompatible with the optical/near-IR imaging. (b) A power-law fit including the effect of the Lyman forest and Lyman valley for a source redshift of z=3.198, again omitting the bin at 5100 Å. The pure power-law fit (a) is rejected at the 98.6% confidence level. The power-law slope of  $\beta=1.32\pm0.25$  resulting from the absorbed model fit (b) is consistent with the slope derived from the optical/near-IR imaging ( $\beta=0.91\pm0.14$ ).

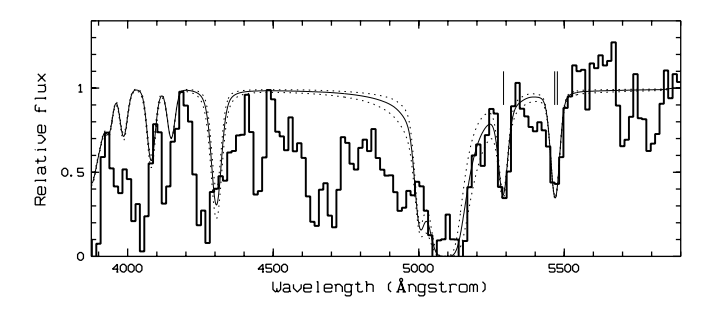


Fig. 4.—FORS1 300V spectrum and model overlay (solid curve) of a z=3.198 damped Ly $\alpha$  line yielding  $\log(N_{\rm H\,I})=21.7\pm0.2$ . The estimated 1  $\sigma$  range is plotted as dotted lines. The model has been fitted to the red wing of the Ly $\alpha$  line and the two lines redward of it. These metal lines, identified as Si II  $\lambda$ 1260 and O I  $\lambda$ 1302 at 5294 and 5468 Å, were used for the redshift determination. For illustrative purposes we also show the region blueward of the Ly $\alpha$  line. This region is dominated by Lyman forest absorption; the data are of very low signal-to-noise ratio. The predicted model is also shown but is not fitted to the data in this region. The data are consistent with the model considering the effect of Lyman forest absorption.

are therefore not useful for a precise redshift determination, and we shall rely only on the Si II  $\lambda 1260$  and O I  $\lambda 1302$  lines at 5294 and 5468 Å for this purpose. The first line is an unblended Si II  $\lambda 1260$  line providing a best-fit redshift of  $3.200 \pm 0.004$ . The O I  $\lambda 1302$  line is blended with a much weaker Si II  $\lambda 1304$  line and provides a redshift of  $3.196 \pm 0.004$ . The combined redshift of these two lines, including wavelength calibration errors, is  $z_{\rm metal} = 3.198 \pm 0.004$ , which we shall adopt as the systemic redshift of the absorber.

Because of the line-blanketing on the blue side of the Ly $\alpha$  line, only the red part of the line profile could be used to constrain the H I column density of the absorber. Within the uncertainty of the redshift, we found that acceptable fits could be obtained in the range  $\log(N_{\rm H\,I})=21.7\pm0.2$ . The estimated 1  $\sigma$  range is marked in Figure 4 by dotted lines.

This column density is among the very highest values observed for QSO DLAs (Storrie-Lombardi & Wolfe 2000). The absorption system is unlikely to be "intervening" (i.e., unrelated to the GRB host) because of the very small probability of such a high column density intervening absorber. More importantly, a significantly higher redshift of the GRB is ruled out by the lack of even stronger Lyman forest absorption redward of 5200 Å (Fig. 3).

#### 3.3. Characteristics of the Optical Decay

In addition to the data presented here, we include the data reported by Berger et al. (2002) to constrain the *R*-band light curve. In Figure 5 we plot all the *R*-band data points versus the logarithm of time since the GRB. The power-law decay index derived from a weighted fit to all the data is  $\alpha=1.64\pm0.03$  [ $f_{\nu}\propto(t-t_{\rm GRB})^{-\alpha}$ ]. This fit is formally rejected with a reduced  $\chi^2/{\rm dof}=26/14$ . Excluding the late-time *HST* data, we derive an acceptable fit with a decay index of  $\alpha=1.49\pm0.04$  and  $\chi^2/{\rm dof}=6/12$ . Fitting only to the data prior to 1 day after the burst, we derive a decay index of  $\alpha=1.45\pm0.06$  with  $\chi^2/{\rm dof}=5/10$ . These results confirm the conclusion of Berger et al. (2002) that the light curve is becoming progressively steeper (a "break"; see Fig. 5).

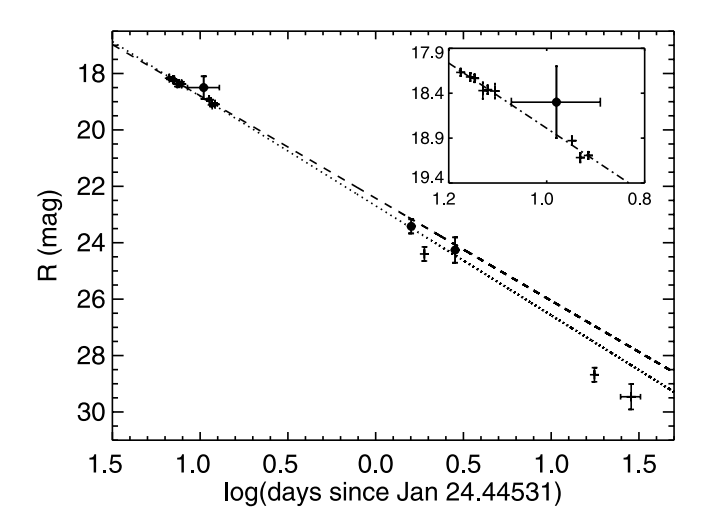


Fig. 5.—*R*-band light curve based on our data (*filled circles*) and from Berger et al. (2002). The dashed line shows a fit to the early data points only. The dotted line is the result of a fit including also the two points from 1 to 3 days after the burst.

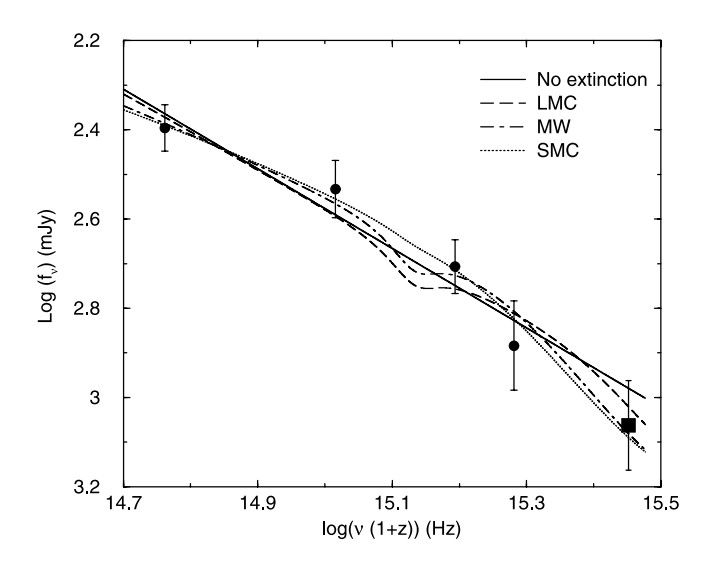


Fig. 6.—BRIJK<sub>s</sub>-band spectral energy distribution of the afterglow on 2003 January 26.20 UT. The filled circles represent the RIJK<sub>s</sub>-band measurements. The filled square is the fiducial B-band photometric point obtained by extrapolating the R-band point using the intrinsic spectral slope ( $\beta = 1.32 \pm 0.25$ ) derived from the VLT spectrum. The fluxes have been corrected for Galactic extinction (Schlegel et al. 1998). The frequencies are given in the rest frame for z = 3.198.

# 3.4. Optical/Near-Infrared SED

Assuming a power-law decay index  $\alpha = 1.49 \pm 0.04$ , we can interpolate the  $RIJK_s$ -band data taken around January 26 UT to a common epoch at January 26.20 2002 UT. After dereddening the contemporaneous  $RIJK_s$ -band points for Galactic extinction (Schlegel, Finkbeiner, & Davis 1998), the colors are  $R-K_s = 2.93 \pm 0.26$  and  $J-K_s = 1.33 \pm 0.20$ . These colors are consistent with the ones expected of a GRB afterglow (see the shaded region of the color-color diagram in Fig. 2 of Gorosabel et al. 2002a).

We have used the intrinsic spectral index obtained from the VLT spectrum ( $\beta=1.32\pm0.25$ ; see § 3.1) to obtain a mock *B*-band point by a power-law extrapolation of the *R*-band measurement. In order to infer information on the extinction [ $A_V$ , E(B-V)], the  $BRIJK_s$ -band SED was fitted with a functional form  $f_{\nu} \propto \nu^{-\beta} \times 10^{-0.4A_{\nu}}$ , where  $A_{\nu}$  is the extinction in magnitudes at rest-frame frequency  $\nu$ .  $A_{\nu}$  was parametrized in terms of  $A_V$  using the three extinction laws reported by Pei (1992), i.e., for the Small Magellanic Cloud (SMC), Large Magellanic Cloud (LMC), and the Milky Way (MW). For comparison purposes we also considered the unextinguished case (pure power-law spectrum given by  $f_{\nu} \propto \nu^{-\beta}$ ).

As shown in Figure 6 and Table 2 (second column), the fits of the three extinction laws are consistent with the data. The derived extinctions are consistent with the no-extinction case (in which case  $\beta = 0.91 \pm 0.14$ ). On the basis

TABLE 2 SED FITTING RESULTS

Extinction Law	$\chi^2/{ m dof}$	E(B-V)	β
MW	1.22	$0.045 \pm 0.101$	$0.69 \pm 0.50$
LMC	0.56	$0.098 \pm 0.079$	$0.29 \pm 0.52$
SMC	0.31	$0.071 \pm 0.051$	$0.31 \pm 0.43$
No extinction	0.78	0	$0.91 \pm 0.14$

of these fits we can set an upper limit of E(B-V) < 0.18. This upper limit, however, corresponds to an unrealistic value of  $\beta$ . Constraining the spectral index to be  $\beta > 0.5$  and the extinction law to be that of the SMC (which provides the best fit to this and most other afterglow SEDs), we find that E(B-V) < 0.065.

#### 4. DISCUSSION

### 4.1. Jet-Wind Fireball Model

Within the framework of the afterglow synchrotron model (Sari, Piran, & Narayan 1998), the decay index,  $\alpha$ , and the spectral index,  $\beta$ , are related through the slope of the electron energy distribution, p. Given the low extinction inferred from the SED analysis, we find that a jet ( $\nu < \nu_c$ , the synchrotron cooling frequency) expanding into a wind medium ( $n \propto r^{-2}$ ) provides the best fireball model for the data. For  $\alpha_1 = 1.49 \pm 0.04$ , this model requires  $p = 2.32 \pm 0.05$  and  $\beta = 0.66 \pm 0.03$ , consistent with the observational results with modest extinction. Expansion into a homogeneous medium ( $\nu < \nu_c$ ) is not strictly ruled out but requires an unusually high value of p: the predicted values are  $p = 2.99 \pm 0.05$  and  $\beta = 1.00 \pm 0.03$  (for  $\alpha_1 = 1.49 \pm 0.04$ ), consistent with the observational values in the absence of extinction.

# 4.2. How Robust is the Redshift Determination?

The spectrum has low resolution and signal-to-noise ratio, but there are five independent pieces of evidence for the redshift. First, assuming a pure power law for the spectrum provides a spectral index of  $2.36 \pm 0.23$ , which is incompatible with  $\beta = 0.91 \pm 0.14$  determined from the photometry. Second, the strong absorption line at 5100 Å cannot be explained by anything other than Ly $\alpha$  at a redshift around 3.2. Third, assuming z = 3.2 and fitting a model with free spectral index, but now including the predicted Lyman forest and valley absorption, one obtains a minimum- $\chi^2$  fit for a spectral index of 1.32  $\pm$  0.25, which is fully compatible with the photometric determination. Fourth, the z = 3.2 fit leads to an improvement in  $\chi^2$  over a single power law alone (for the same dof) that rejects the single power law at the 98.6% level. Fifth, there are two identified metal lines, and none of the lines predicted from the explicit fit (e.g., Ly $\beta$ ) are inconsistent with the observed spectrum (Fig. 4).

### 4.3. Dim or Bright?

The fact that GRB 020124 was a fairly dim burst (Berger et al. 2002), but fitted by a normal fireball model without excessive extinction, reinforces the conclusion of Hjorth et al. (2002; GRB 980613), Berger et al. (2002; GRB 020124), and Fox et al. (2003; GRB 021211) that there

is a population of dim, unextinguished GRB afterglows that can account for at least some of the large fraction of ("dark") bursts for which no optical afterglow is detected (Fynbo et al. 2001a). In the case of GRB 020124 this is mainly due to the fairly high redshift (unlike GRB 980613 and GRB 021211, which are at redshifts 1.096 [Djorgovski et al. 1999] and 1.006 [Vreeswijk et al. 2003a], respectively): If an afterglow is redshifted from  $z_1$  to  $z_2$ , it is dimmed by

$$\Delta \mu + 2.5(\beta - \alpha - 1) \log [(1 + z_2)/(1 + z_1)]$$
.

For a median GRB redshift of  $z_1 = 1$  and  $z_2 = 3.198$  the relative dimming amounts to 1.82 mag (for  $\alpha = 1.49$  and  $\beta = 0.91$ ). If the afterglow had been 1.82 mag brighter, it would have been a typical bright afterglow:  $R \approx 16.7$  after 2 hr and  $R \approx 20.7$  after 1 day (see, e.g., Fig. 3 of Gorosabel et al. 2002b or Fig. 2 of Fox et al. 2003).

# 4.4. N(H I) versus E(B-V)

The Galactic relation between the column density of neutral hydrogen and the reddening is N(H I)/E(B-V) = $4.93 \pm 0.28 \times 10^{21}$  cm<sup>2</sup> mag<sup>-1</sup> (Diplas & Savage 1994). For the LMC and SMC the corresponding ratios are  $N({\rm H~{\sc i}})/E(B-V) = 2 \pm 0.5 \times 10^{22} {\rm cm^2~mag^{-1}}$  and  $N({\rm H~{\sc i}})/E(B-V) = 4.4 \pm 0.7 \times 10^{22} {\rm cm^2~mag^{-1}}$ , respectively (Koornneef 1982; Bouchet et al. 1985). In Table 3 we list this ratio for known GRBs for which the H I column density and E(B-V) have been measured or constrained from optical spectroscopy and optical/near-infrared photometry (the values given are for an SMC extinction law). In addition to GRB 020124, these are GRB 000301C (Jensen et al. 2001) and GRB 000926 (Fynbo et al. 2001b, 2001c). We exclude GRB 021004, which has several intervening absorbers at different redshifts. It is evident that the values for N(H I)E(B-V) are not larger than expected for galaxies like the LMC or SMC. Taken at face value these results indicate that the GRB surroundings are low in dust, because of low metallicity (e.g., for a universal dust-to-metals ratio) and/or because of a low dust-to-metal ratio (a large fraction of the metals being in the gas phase). This conclusion is fully consistent with what is found in QSO DLAs (Pettini et al. 1997a).

It has been suggested that the intense UV and X-ray flux from a GRB may photoionize the surrounding gas and destroy dust grains (Waxman & Draine 2000; Fruchter, Krolik, & Rhoads 2001; Perna & Lazzati 2002), resulting in changes in the derived  $N(H\ I)$ ,  $A_V$ , E(B-V), and their ratios. Galama & Wijers (2001) studied the inferred absorption of soft X-rays in BeppoSAX GRB afterglows and compared it with the optical extinction as inferred from a fireball model fit to the available data. They claimed evidence for a high  $N(H\ I)/A_V$  ratio and concluded that dust destruction may be the cause. The most convincing case for dust destruction along these lines was made by Galama

TABLE 3
COLUMN DENSITY AND REDDENING FOR GRB ABSORBERS

GRB	Z	log N(H I)	E(B-V) (mag)	$N({\rm H~I})/E(B-V)$ (10 <sup>21</sup> cm <sup>2</sup> mag <sup>-1</sup> )	Reference
000301C 000926 020124	2.040 2.038 3.198	$21.2 \pm 0.5$ $21.3 \pm 0.2$ $21.7 \pm 0.2$	$\begin{array}{c} 0.031 \pm 0.014 \\ 0.062 \pm 0.020 \\ < 0.065 \end{array}$	$51^{+113}_{-42} \\ 32^{+21}_{-16} \\ > 49$	Jensen et al. 2001 Fynbo et al. 2001b, 2001c This paper

et al. (2003), who found a high value of  $N({\rm H~{\sc i}})/A_V$  for GRB 010222, based on *Chandra X-Ray Observatory* data. At the same time they interpreted a strong (i.e., nongray) farultraviolet (rest-frame wavelength ~1100 Å) component in the extinction of GRB 010222 as evidence for dust destruction.

In a comparison of the properties of DLAs and GRB absorbers, Savaglio, Fall, & Fiore (2003) claimed that GRB 990123 (z=1.60), GRB 000926 (z=2.04), and GRB 010222 (z=1.48) [of which only GRB 000926 has a measured  $N(H\ I)$ ; Fynbo et al. 2001b] have higher metal column densities and contain more dust than DLAs at similar redshifts. They further suggested that the relatively low reddening (rest-frame wavelength >1200 Å) observed toward these GRBs may be due to a gray extinction law, produced by dust destruction (Perna, Lazzati, & Fiore 2003).

Castro et al. (2003) argue that the chromium-to-zinc ratio toward GRB 000926 indicates that the host is depleted in dust relative to local values to a similar degree as QSO DLAs at the same redshift. This conclusion is consistent with what we have suggested above for GRB 020124, namely, that the GRB surroundings have a low dust-to-gas ratio, similar to QSO DLAs (Pettini et al. 1997a). An additional argument in favor of this interpretation is that a significant amount of gray extinction would make the afterglow intrinsically even brighter than indicated above (§ 4.3). For example, assuming a Galactic value of  $N(H I)/A_V$ ,  $\log N(\text{H I}) = 21.7$ , destruction of two-thirds of the dust producing the extinction in the rest-frame V band (Perna et al. 2003) and a flat extinction curve would dim the afterglow by 1 mag. Any nongray component would significantly increase this value.

We conclude that the high value of the ratio between column density and optical extinction first found by Galama & Wijers (2001) from X-ray spectroscopy remains when N(H I) is estimated from optical spectroscopy in GRB afterglows with a DLA host and the extinction is estimated from the observed reddening of the optical/NIR afterglow. The dust destruction interpretation originally proposed by Galama & Wijers (2001) to account for the X-ray result could conceivably also be applied in this case. The observed small reddening would be due to a modification of the extinction law due to preferential destruction of small grains by the prompt UV and X-ray radiation from the GRB, leading to a gray extinction law. However, we have found that the straightforward alternative explanation, namely, that GRBs occur in less chemically enriched environments, similar to those of the SMC and QSO DLAs, is fully consistent with the optical observations reported here.

Future joint optical and X-ray spectroscopy of  $1.6 \lesssim z \lesssim 2.5$  GRBs combined with accurate multiwavelength observations of the afterglow, in particular in the optical/NIR regime, can be used to distinguish between these two possibilities and at the same time fix the metallicity of the burst environment.

We thank Jochen Greiner, Sylvio Klose, and Kristian Pedersen for useful comments. J. P. U. F. acknowledges support from the Carlsberg Foundation. J. M. C. C acknowledges the receipt of a FPI doctoral fellowship from Spain's Ministerio de Ciencia y Tecnología. The authors acknowledge benefits from collaboration within the EU FP5 Research Training Network "Gamma-Ray Bursts: An Enigma and a Tool." This work was also supported by the Danish Natural Science Research Council (SNF).

#### REFERENCES

```
Andersen, M. I., et al. 2000, A&A, 364, L54
Berger, E., et al. 2002, ApJ, 581, 981
Bessel, M. S. 1990, PASP, 102, 1181
Bloom, J. S., Kulkarni, S. R., & Djorgovski, S. G. 2002, AJ, 123, 1111
Bouchet, P., Lequeux, J., Maurice, E., Prevot, L., & Prevot-Burnichon,
   M. L. 1985, A&A, 149, 330
Castro, S., Galama, T. J., Harrison, F. A., Holtzman, J. A., Bloom, J. S.,
   Djorgovski, S. G., & Kulkarni, S. R. 2003, ApJ, 586, 128
Devillard, N. 1997, Messenger, 87, 19
Diplas, A., & Savage, B. D. 1994, ApJ, 427, 274
Djorgovski, S. G., Kulkarni, S. R., Bloom, J. S., Frail, D., Chaffee, F., & Goodrich, R. 1999, GCN Circ. 189
Djorgovski, S. G., Pahre, M. A., Bechtold, J., & Elston, R. 1996, Nature,
Fox, D. W., et al. 2003, ApJ, 586, L5
Fruchter, A. S., Krolik, J. H., & Rhoads, J. E. 2001, ApJ, 563, 597
Fynbo, J. P. U., Møller, P., & Warren, S. J. 1999, MNRAS, 305, 849
Fynbo, J. P. U., et al. 2001a, A&A, 369, 373
   2001b, in Lighthouses of the Universe: The Most Luminous Celestial Objects and Their Use for Cosmology (Garching: Springer),
   187
——. 2001c, A&A, 373, 796
Galama, T. J., & Wijers, R. A. M. J. 2001, ApJ, 549, L209
Galama, T. J., et al. 2003, ApJ, 587, 135
Gorosabel, J., et al. 2002a, A&A, 384, 11
           2002b, A&A, 383, 112
Hamuy, M., Suntzeff, N. B., Heathcote, S. R., Walker, A. R., Gigoux, P., &
   Phillips, M. M. 1994, PASP, 106, 566
Henden, A. 2002, GCN Circ. 1251
Hjorth, J., et al. 2002, ApJ, 576, 113
Jensen, B. L., et al. 2001, A&A, 370, 909
```

```
Koornneef, J. 1982, A&A, 107, 247
Kulkarni, V. P., Fall, S. M., & Truran, J. W. 1997, ApJ, 484, L7
Ledoux, C., Bergeron, J., & Petitjean, P. 2002, A&A, 385, 802
Lu, L., Sargent, W. L. W., Barlow, T. A., Churchill, C. W., & Vogt, S. S. 1996, ApJS, 107, 475
Møller, P., & Jakobsen, P. 1990, A&A, 228, 299
Møller, P., & Warren, S. J. 1993, A&A, 270, 43
——————. 1998, MNRAS, 299, 661
Møller, P., Warren, S. J., Fall, S. M., Fynbo, J. P. U., & Jakobsen, P. 2002,
ApJ, 574, 51
Pei, Y. C. 1992, ApJ, 395, 130
Pei, Y. C., Fall, S. M., & Bechtold, J. 1991, ApJ, 378, 6
Perna, R., & Lazzati, D. 2002, ApJ, 580, 261
Perna, R., Lazzati, D., & Fiore, F. 2003, ApJ, 585, 775
Persson, S. E., Murphy, D. C., Krzeminski, W., Roth, M., & Rieke, M. J.
   1998, AJ, 116, 247
Pettini, M., King, D. L., Smith, L. J., & Hunstead, R. W. 1997a, ApJ, 478,
   536
Pettini, M., Smith, L. J., King, D. L., & Hunstead, R. W. 1997b, ApJ, 486,
Ricker, G. R., et al. 2002, GCN Circ. 1220
Sari, R., Piran, T., & Narayan, R. 1998, ApJ, 497, L17
Savaglio, S., Fall, S. M., & Fiore, F. 2003, ApJ, 585, 638
Schlegel, D. J., Finkbeiner, D. P., & Davis, M. 1998, ApJ, 500, 525
Storrie-Lombardi, L. J., & Wolfe, A. M. 2000, ApJ, 543, 552
Vreeswijk, P., Fruchter, A., Hjorth, J., & Kouveliotou, C. 2003a, GCN
   Circ. 1785
Vreeswijk, P., Wijers, R., Rol, E., & Hjorth, J. 2003b, GCN Circ. 1953
Waxman, E., & Draine, B. T. 2000, ApJ, 537, 796
Wolfe, A. M., Turnshek, D. A., Smith, H. E., & Cohen, R. D. 1986, ApJS,
```